Article

Simultaneous High-resolution Detection of Bioenergetic Molecules using Biomimetic-receptor Nanopore

zhuoqun su, Yongfeng Wei, and Xiaofeng Kang

Anal. Chem., **Just Accepted Manuscript** • DOI: 10.1021/acs.analchem.9b04268 • Publication Date (Web): 30 Oct 2019

Simultaneous High-resolution Detection of Bioenergetic Molecules using Biomimetic-receptor Nanopore

Zhuoqun Su, Yongfeng Wei and Xiaofeng Kang*

Key Laboratory of Synthetic and Natural Functional Molecular Chemistry, College of Chemistry & Materials Science, Northwest University, Xi'an 710069, P. R. China

ABSTRACT: A novel artificial receptor, heptakis-[6-deoxy-6-(2-hydroxy-3-trimethylammonion-propyl) amino]-beta-cyclomaltoheptaose, with similar functions of mitochondrial ADP/ATP carrier protein, was synthesized and harboured in the engineered α-HL $(M113R)_7$ nanopore, forming single-molecule biosensor for sensing bioenergetic molecules and their transformations. The strategy significantly elevates both selectivity and signal-to-noise, which enables to simultaneously recognize and detect ATP, ADP and AMP by real-time single-molecule measurement.

Single-molecule analysis has unique advantages over ensemble or bulk-measurement in detecting species, which can simultaneously provide fingerprint information of not only single molecule, but also many different single molecules by molecular counting.[1] Such ability to capture the characteristic detail of sample heterogeneity is very important on biological applications, especially in the detections of complex biofluid and/or those components with minor differences. For example, adenosine-5'-triphosphate (ATP), adenosine-5'-diphosphate (ADP) and adenosine-5'-monophosphate (AMP) (referred to as adenosine phosphates, APs) that are relevant to biological energy storage and signal transduction[2] have recently also designated as noninvasive diagnostic and prognostic biomarkers for many diseases including Alzheimer, Parkinson and those involving the heart and blood vessels.[3-5] To obtain insight into the important and complex cell energy-relevant biological processes and to meet clinical needs, there is a growing demand to simultaneously detect them, but is an extreme challenge because of similar structures, fast and reversible conversion between them under specific catalysis of enzymes[6] as well as wider distribution (ATP level for healthy cell: 0.28 pM-11 pM per cell).[7]

Among many various single-molecule methods available at present, nanopore technology has emerged as a powerful tool to treat biological problems due to simplicity, label-free, solution-based detection and easy operation.[8–13] The technology mainly replies on the changes in nanopore current produced by analyte-translocating events. Therefore, protein nanopore, unlike with solid nanopore, should have a top priority in sensing small molecules because of comparable dimensions. But, in recognizing and capturing small biomolecule, effective nanopore including the most commonly used α-hemolysin (α-HL) has remained remarkably unpredictable, which could be resulted from the fast transport through nanopore[14] and its own properties of lacking selectivity[15]. Some efforts have addressed above limitations by (1) functionalizing the nanopore surface with hydrophobic[16], and positively[17] or negatively[18] charged residues; (2) modifying[19] or carrying analyte[20-22]. These strategies are cumbersome, require careful optimization, yet frequently are ineffective. It is still an essential challenge to develop reliable nanopore that is able to distinguish and detect directly specific molecules such as ATP, ADP and AMP, with high selectivity and sensitivity. For this purpose, bio-inspired strategy could be a perfect solution. Herein, we display that such biomimetic receptor (BR)-equipped protein nanopore can be obtained by two-step processes: (1) designing and synthesizing a new artificial receptor that resembles mitochondrial ADP/ATP carrier protein in the shape and the vital functional residues; (2) followed by binding it in the engineered α-HL $(M113R)_7$ to form single-molecule sensing element. We demonstrate its excellent performance through the molecular simulation and the single-molecule electronic measurements in both recognizing APs simultaneously and real-time enzyme-catalyzing transformation kinetics and thermodynamics. Furthermore, the ability at the single-phosphate resolution has also great promise in synthetic DNA sequencing.[23]

EXPERIMENTAL SECTION

Reagents and Materials. adenosine-5'-triphosphate (ATP, 99%), adenosine-5'-diphosphate (ADP, 99%) and adenosine-5'-monophosphate (AMP, 99%), 2, 3-epoxypropyl trimethylammonium chloride (95%) and calf intestinal alkaline phosphatase (CIALP, EC 3.1. 3.1) were purchased from Sigma-Aldrich. 1,2-Diphytanoyl-*sn*-glycero-3-phosphocholine was obtained from Avanti Polar Lipids, The thickness of Teflon film (Goodfellow) was 25 μm.

Single-Channel Recording and Data Analysis. 2-Diphytanoylphosphatidylcholine (DPhPC) bilayer was formed over a 130~150 μm aperture in a Teflon septum that divided a planar bilayer chamber into cis and trans parts. Both solutions were 1 M KCl and buffered with 10 mM Tris (pH 7.5). $(M113R)_7$, ATP, ADP, AMP and enzyme CIALP were added to the cis compartment that was connected to the ground. BR was added to the trans side that was connected to the head-stage of the amplifier. The final concentration of the $(M113R)_7$ proteins was 0.08–0.18 ng/mL. Currents were recorded with a patch clamp amplifier (Axopatch 200B, Molecular Devices, Sunnyvale, CA), filtered with a four-pole Bessel filter at 5 kHz, sampled at 100 kHz by a computer equipped with a Digidata 1550 A/D converter (Molecular Devices), and acquired with Clampex 10.4 software (Molecular Devices). Single-channel events were analyzed using Clampfit 10.5 (Molecular Devices) and origin 9.0 (Microcal, Northampton, MA) software. Mean dwell time values were obtained from the dwell histograms that were fitted to single exponential functions. The blockades were plotted as residual current histograms and the distributions were fitted to Gaussian functions.

RESULTS AND DISCUSSION

Design and synthesis of biomimetic receptor. The key of mitochondrial ADP/ATP carrier protein to recognize and transport ADP/ATP is the five positively charged arginine (R) residues (R79, R137, R234, R235 and R279) in its funnel-shaped cavity, forming a high-density charge cluster (Fig.1a).[24] Inspired by the specific structure, we designed and synthesized a biomimetic receptor (BR), (heptakis-[6-deoxy-6-(2-hydroxy-3-trimethylammonion-propyl)amino]-beta-cyclomaltoheptaose) (Fig.1b), containing a cluster of positively charged quaternary ammoniums that is permanently charged, and independent on the solution pH.[25] Cyclomaltoheptaose is a bowl-like hollow molecule with 6.0-6.5 Å in diameter.[26] The cavity size is comparable with the size of the mitochondrial ADP/ATP carrier (about 8Å in diameter)[24] and well matches ATP/ADP/AMP molecules (maximum size 6 Å).[27] The BR was prepared by four-step reactions: The first three-step reactions were to convert all the primary hydroxyl groups of β-cyclomaltoheptaose to amino groups (SI 2 and Fig. S1); the heptakis-(6-deoxy-6-amino)-β-cyclomaltoheptaose subsequently underwent the chemical reaction with 2, 3-epoxypropyl trimethylammonim chloride in triethylamine-HCl buffer solution (pH=10) at 50 °C for 24 hours (Fig. 1c). The final BR product (yield: 51%) was characterized by ESI-MS (m/z): $[M]^{7+}$ = 277.1822.

Interactions between BR and APs. As we previously reported, the quaternary ammonium cation is distinctive for binding DNA derivatives,[12,28] so the ring of high-density quaternary ammonium cations located in the funnel bottom of the BR could be utilized as a molecular trap to catch adenosine phosphate derivatives. The predefined property was demonstrated by forming BR-APs complexes in bulk solution (Details see SI Fig. S4a-f, Table S1-4 and S9).Through the measurements of UV-visible absorbance (ΔA) of APs at 260 nm, we observed the obvious differences of three complexes in the formation constant (K_f) and the standard free energy ($\Delta G°$): K_f (BR-ATP) =1.02×10⁴ M⁻¹, K_f (BR-ADP)=2.18×10⁴ M⁻¹, K_f (BR-AMP)= 6.87×10⁴ M⁻¹, $\Delta G°$ (BR-ATP) = -27.11 kJ mol⁻¹, $\Delta G°$ (BR-ADP)= -24.34 kJ mol⁻¹ and $\Delta G°$ (BR-AMP)= -22.46 kJ mol⁻¹ at 20 °C , which should be ascribed to both various phosphate number and chain length (see SI 3).

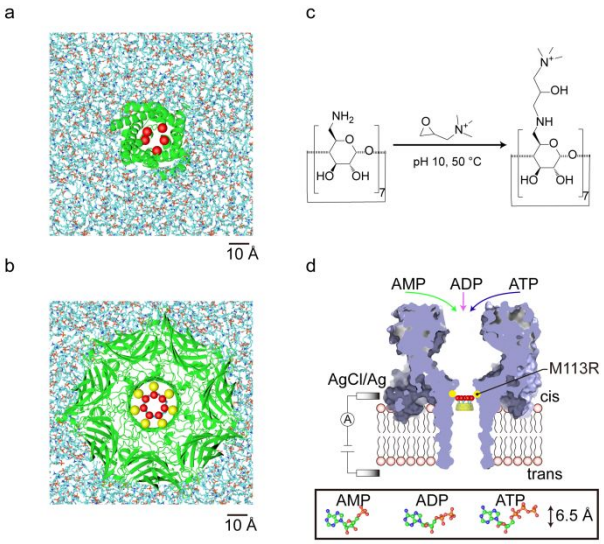

Figure 1. Construction of biomimetic receptor-equipped protein nanopore. (a) The top view of the mitochondrial ADP/ATP carrier inserted into lipid bilayer (POPC, 110 Å×110 Å). The cationic cluster consisting of five arginine residents (R79, R137, R234, R235, R279) in the ADP/ATP carrier is represented by red balls. (b) The molecular model of biomimetic receptor-equipped $(M113R)_7$ nanopore in the lipid bilayer (POPC, 110 Å×110 Å). BR is located in the barrel of a mutated M113R α-HL pore (R is labeled by yellow color). The quaternary ammonium of BR is represented by red color. (c) The synthesis of heptakis-[6-deoxy-6-(2-hydroxy-3-trimethylammonio-n-propyl) amino]-cyclomaltoheptaose (BR) from heptakis-(6-deoxy-6-amino)-cyclomaltoheptaose, which was treated with 2, 3-epoxypropyl trimethylammonium chloride in triethylamine-HCl buffer solution (pH=10) at 50 °C for 24 hours. (d) Schematic representation of the APs detection system using BR-equipped $(M113R)_7$ α-HL pore. BR was added into the *trans* side and APs to the *cis* side. Structural models of mitochondrial ADP/ATP carrier and α-HL were produced by PDB 2C3E and PDB 7AHL, BR, APs and POPC lipids were constructed and then rendered by VMD and PyMOL software.

We further investigated the interaction of BR and APs using molecular docking simulation analysis (Details see SI 4). The results of semi-flexible docking approaches revealed that ATP, ADP and AMP as guest molecule all exhibited high affinity with host molecule BR (SI, Fig.S5). However, the number of salt bridge between ammonium groups and phosphates (SI, Table S5-7) was gradually reduced in these 1:1 complexes: 5 (ATP-BR), 4 (ADP-BR) and 3 (AMP-BR), while the number of hydrogen bonds

was also reduced: 7 (ATP-BR), 5 (ADP-BR) and 4 (AMP-BR).

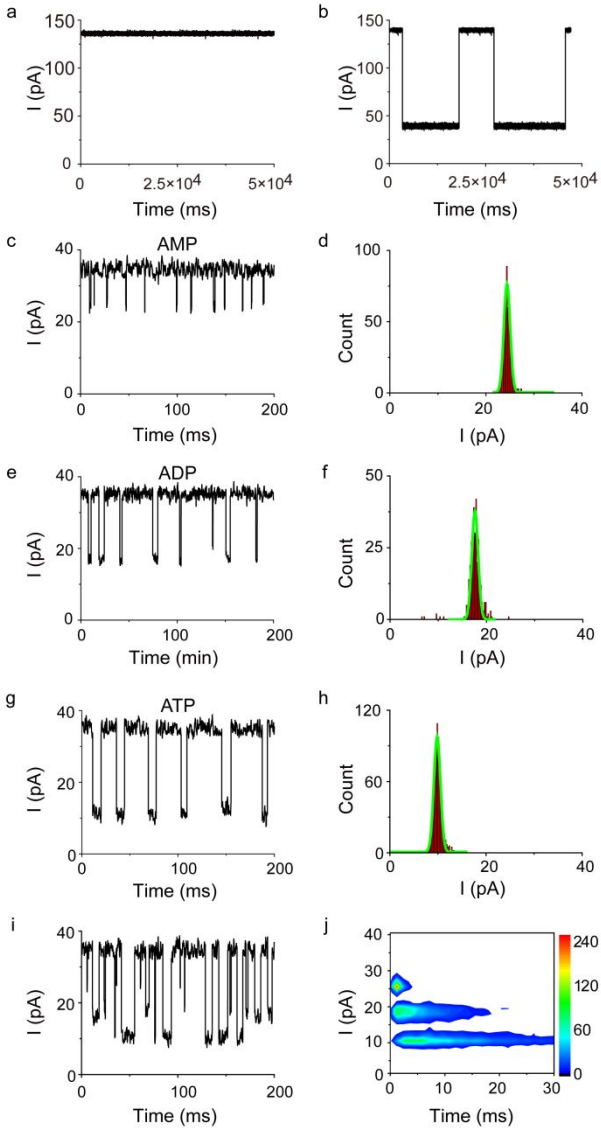

Figure 2. $(M113R)_7$-BR nanopore for sensing APs. Typical current traces recording at 140 mV with (a) $(M113R)_7$ pore, (b) $(M113R)_7$-BR pore, and $(M113R)_7$-BR pore for (c) AMP, (e) ADP, (g) ATP, (i) the mixture of ATP, ADP and AMP. The residual current histograms: AMP (d), ADP (f) and ATP (h). (j) 2D contour plot of the APs mixture. The concentration of APs (Cis side): ATP (1.78 μM), ADP (5.35 μM) and AMP (7.12 μM). The concentration of BR is 60 μM (Trans side). The experiment temperature is 20 °C.

Single-molecule recognition and detection of APs. We prepared genetically engineered α-hemolysin protein pore, $(M113R)_7$ and mounted BR molecule at 113 binding sites, forming single-molecule recognition and detection device (Fig. 1d). The $(M113R)_7$ pore produced a stable opening current. When +140 mV voltage was applied, single-channel current was 140±5 pA (n=24) in 1 M KCl (Fig.2a). For the bound-BR $(M113R)_7$ pore, $(M113R)_7$-BR, only a 36±2 pA (n=15) current level was observed at +140 mV (Fig.2b). The mutants of the $(M113R)_7$ pore that bind the BR molecule is ~10^3 times more tightly than the wild-type pore that binds cyclomaltoheptaose molecule (SI Table S8). Next, we tested the recognizing ability of the $(M113R)_7$-BR pore for APs by single-channel recording. After adding to the cis side (on the opposite side of the BR), ATP, ADP and AMP exhibited three distinct current-blocking levels: 10.38±1.35 pA (n=26) for ATP, 18.68±1.58 pA (n=20) for ADP and 24.76±1.69 pA (n=19) for AMP, at +140 mV, respectively (Fig.2c-h). Despite only one phosphate difference, the current value varies greatly at least 6.08 pA. Such a huge difference is especially important for quickly distinguishing them through direct readout. We also note that two differences in current between ATP-ADP and ADP-AMP (6.08 pA and 8.3 pA) is not equal, which means that the current change resulted from APs in $(M113R)_7$-BR pore is not only size-exclusion effect, but also deals with different conformation of ATP, ADP and AMP. This subtle difference can also be observed in docking results. The mean dwell time (τ_{off}) values for di-anion AMP with monophosphate, tri-anion ADP with biphosphate, or tetra-anion ATP with triphosphate were 0.64±0.03 ms (n=26), 3.87±0.36 ms (n=21) and 7.34±0.90 ms (n=19), respectively. The longer dwell time reflects the stronger binding. These results demonstrated that the interaction between APs and $(M113R)_7$-BR is highly dependent on the number of their charges and number of hydrogen bonds. To evaluate the distinguishing ability in mixture, the mixture of ATP, ADP and AMP was added to the cis side and three current levels quickly arose in the current traces, which is clearly visible with naked eye (Fig. 2i). As shown in the 2D-contour plot (Fig. 2j), the current values and the dwell time of them in the mixture are the same as that in the individual substance. However, mixture of ATP, ADP and AMP for $(M113R)_7$ was unable to be discriminated. APs could not introduce any signal for WT α-hemolysin (see SI Figure S8).

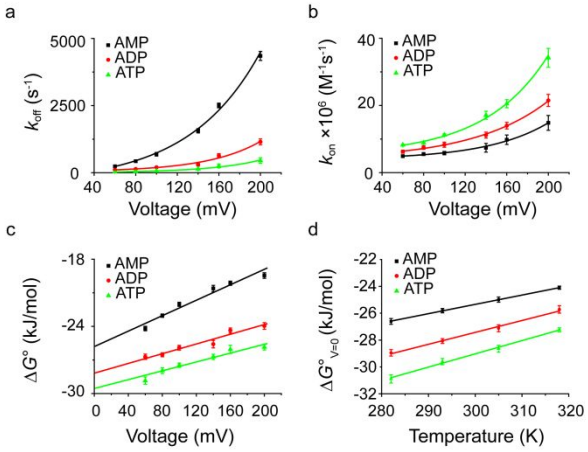

Figure 3. The interactions between APs and $(M113R)_7$-BR. (a-b) the plots of the k_{off} ~V and k_{on}~V. (c) The voltage (V) dependence of the standard free energy ($\Delta G°$). (d) Variation of standard free energy ($\Delta G°$) at different temperatures. APs: AMP (black color), ADP (red color) and ATP (green color).

Enthalpy-driven the binding of APs in the confined nanopore. The binding of APs in $(M113R)_7$-BR pore is voltage-dependent. The rate constants at different voltages were obtained and analyzed as previously described.[29] Although both the association constant k_{on} ($1/c^*\tau_{on}$) and the dissociation constant k_{off} ($1/\tau_{off}$) of APs in the $(M113R)_7$-BR pore exponentially increase with increasing voltage (Fig. 3a,b), the standard free energy $\Delta G°$ ($\Delta G° = -RT\ ln((k_{on})/(k_{off}))$) linearly increases (Fig. 3c), suggesting the decrease in the stability of $(M113R)_7$-BR-APs complexes or the reduction of the binding frequency with increasing voltage. By extrapolating the linear relationship between $\Delta G°$ and the voltage, the standard free energy ($\Delta G°_{V=0}$) values at 0 mV are gained: -25.81 kJ mol^{-1} for AMP, -28.07 kJ mol^{-1} for ADP and -29.6 kJ mol^{-1} for ATP, respectively. The $\Delta G°_{V=0}$ values decrease linearly as the temperature increases (Fig. 3d). The values of $\Delta H°$ and $\Delta S°$ obtained by linear fitting of $\Delta G°_{V=0}$ and temperature (T) are -46.41±0.42 kJ mol^{-1} and -70.27±1.46 J mol^{-1} for AMP, -53.99±1.47 kJ mol^{-1} and -88.55 ± 2.32 J mol^{-1} for ADP, as well as -58.63±1.26 kJ mol^{-1} and -98.69±4.11 J mol^{-1} for ATP. Both $\Delta H°$ and $\Delta S°$ are negative. However, the huge enthalpy change ($\Delta H°$) that can completely offset the small change in $T\Delta S°$, produces a larger negative value of $\Delta G°_{V=0}$, thus making the binding of APs to proceed spontaneously and favorably. The overall exothermic binding in the confined space is mainly an enthalpy-driven process. Interestingly, $\Delta G°_{V=0}$ in the $(M113R)_7$-BR nanopore is more negative in compared with $\Delta G°$ in the bulk solution (SI Table S9). For ATP, ADP and AMP, the difference in the standard free energy is $\Delta\Delta G°_{ATP}$ =-2.49 kJ mol^{-1}, $\Delta\Delta G°_{ADP}$=-3.73 kJ mol^{-1} and $\Delta\Delta G°_{AMP}$= -3.35 kJ mol^{-1}, respectively, demonstrating that the binding in the $(M113R)_7$-BR nanopore is more favorable. The $\Delta\Delta G°$ should be ascribed to the space effect in confined nanopore.

Real-time monitoring enzyme-catalyzing transformation. Based on the method above, the process of the ATP hydrolysis catalyzed by calf intestinal alkaline phosphatase (CIALP, EC 3.1. 3.1) was monitored (Fig. 4a). In the absence of CIALP, ATP produced only the events with 10.38±1.35 pA level at 140 mV voltage (Fig. 4b, 4g). After adding CIALP in the ATP solution, the ADP and AMP signals (18.68±1.58 pA level and 24.76±1.69 pA level) accompanying with ATP signal were generated in 2 hours continuous recording (Fig. 4c-f and 4h-j). The frequency of events (f) or the event number of unit time for each substance changed over time is proportional to its concentration(C), $C=k_{on}^{-1}\bullet f$. By fitting the scatter plot by kinetic equation, the time-resolved change in the concentration of ATP, ADP and AMP was directly obtained by monitoring ATP, ADP and AMP signals (Fig. 4k). Upon adding CIALP, ATP concentration drops sharply from 7.4 μM to nearly 2 μM within 30 min and followed by a slow process to zero, while ADP and AMP increase first, then decrease, with the maximum peaks at 2.8±0.3 μM/25min and 1.9±0.2 μM/50min, respectively, and finally convert to adenosine by sigmoid relationship, which does not produce any current-blocking response. The fitted apparent hydrolysis rate constants of ATP, ADP, and AMP were 0.047 min^{-1}, 0.050 min^{-1} and 0.063 min^{-1}, respectively (see SI 6), indicating the hydrolysis ability of CIALP for APs: AMP > ADP > ATP. This sequence is in accordance with alkaline phosphatase from other sources.[30] Fig.4l is the scatter plot of all events during whole enzyme-catalyzing transformation. We clearly observed (i) three kinetic phases by simultaneous monitoring ATP, ADP and AMP using biomimetic-receptor nanopore; (ii) that three kinetic phases take place in a time sequential fashion; and (iii) different point density (or blackness) in the time-course of ATP hydrolysis, which represents their concentrations.

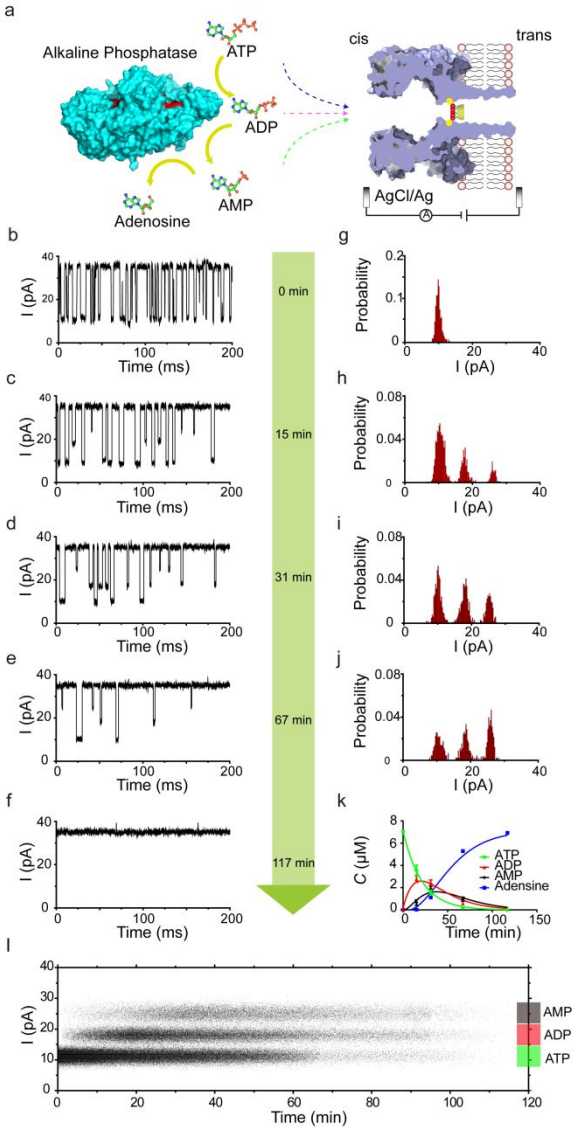

Figure 4. ATP hydrolysis kinetics and analysis. (a) Schematic representation of detecting ATP hydrolysis process. ATP hydrolysis was catalyzed by enzyme calf intestinal alkaline phosphatase (CIALP, EC 3.1.3.1). The structure of alkaline phosphatase is from PDB 1B8J and active sites are represented by red colour. (b-f) Representative current-time traces at 0, 15 min, 31 min, 67 min and 117 min, respectively. The hydrolysis of ATP (7.4 μM) was conducted by adding

CIALP (0.89 unit/mL activated by 25 nM Mg^{2+} and 2.5 nM Zn^{2+}) to the cis side. (g-j) The normalized histogram plots of the residual current at different times. (k) The concentration variations of APs and adenosine during the hydrolysis process. Averaged adenosine concentration was calculated by the formula: 7.04 - ([ATP] + [ADP] + [AMP]). (l) The scatter plot of all events during enzyme-catalyzing transformation. The hydrolysis was conducted in solution of 1 M KCl, 10 mM Tris-HCl, pH=7.5, at 20 °C. The applied voltage was 140 mV.

CONCLUSIONS

BR-nanopore assay here described is a single-molecule approach to detect bioenergetic molecules and their transformations, which has many potential advantages: (i) the high selectivity of BR allows BR-nanopore to effectively capture and identify ATP, ADP and AMP; (ii) It is label-free, no amplification and no modification so does not suffer from other interference; (iii) the high-resolution real-time signals for ATP, ADP and AMP enable us to directly read out their information; (iv) the ability for simultaneous rapid monitoring of ATP, ADP and AMP is hard to achieve by other methods. Although simultaneous analyzing bioenergy-related molecules and their transformation dynamics has been demonstrated, BR-nanopore strategy is broadly useful to any involved-phosphate biological processes and application, for example, synthetic DNA sequencing method,[23,31] detecting phosphorylation of DNA/RNA and protein[32-34].

ASSOCIATED CONTENT

Supporting Information

This material is available free of charge via the Internet at http://pubs.acs.org. Experimental details describing the synthesis, characterization, detailed information on molecular simulation, and analysis on hydrolysis kinetics, as well as additional figures.

AUTHOR INFORMATION

Corresponding Author

* kangxf@nwu.edu.cn

Notes

The authors declare no competing financial interest.

ACKNOWLEDGMENT

This work was financially supported by the National Science Foundation of China (NSFC: 21375104, 21327806 and 21874107).

REFERENCES

(1) Gooding, J. J.; Gaus, K. *Angew. Chem. Int. Ed.* **2016**, *55*, 11354-11366.

(2) Knowles, J. R. *Annu. Rev. Biochem.* **1980**, *49*, 877-919.

(3) Yokoshiki, H.; Sunagawa, M.; Seki, T.; Sperelakis, N. *Am. J. Physiol.-Cell Physiol.* **1998**, *274*, C25-C37.

(4) Przedborski, S.; Vila, M. *Clin. Neurosci. Res.* **2001**, *1*, 407-418.

(5) Annunziato, L.; Pignataro, G.; Di Renzo, G. F. *Pharmacol. Rev.* **2004**, *56*, 633-654.

(6) Eaton, R. H.; Moss, D. W. *Biochem. J.* **1967**, *104*, 65.

(7) Mikirova, N.; Riordan, H. D.; Kirby, R. K.; Klykov, A.; Jackson, J. A. *J. Orthomol. Med.* **2005**, *20*, 50-58.

(8) Clarke, J.; Wu, H.-C.; Jayasinghe, L.; Patel, A.; Reid, S.; Bayley, H. *Nat. Nanotechnol.* **2009**, *4*, 265.

(9) Derrington, I. M.; Butler, T. Z.; Collins, M. D.; Manrao, E.; Pavlenok, M.; Niederweis, M.; Gundlach, J. H. *Proc. Natl. Acad. Sci.* **2010**, *107*, 16060-16065.

(10) Yao, F.; Zhang, Y.; Wei, Y.; Kang, X. *Chem. Commun.* **2014**, *50*, 13853-13856.

(11) Ramsay, W. J.; Bayley, H. *Angew. Chem. Int. Ed.* *57*, 2841-2845.

(12) Wang, Y.; Yao, F.; Kang, X. F. *Anal. Chem.* **2015**, *87*, 9991-9997.

(13) Tan, C. S.; Fleming, A. M.; Ren, H.; Burrows, C. J.; White, H. S. *J. Am. Chem. Soc.* **2018**, *140*, 14224-14234.

(14) Carson, S.; Wanunu, M. *Nanotechnology* **2015**, *26*, 1-14.

(15) Howorka, S. *Nat. Nanotechnol.* **2017**, *12*, 619.

(16) Guan, X.; Gu, L. Q.; Cheley, S.; Braha, O.; Bayley, H. *ChemBioChem* **2005**, *6*, 1875-1881.

(17) Maglia, G.; Restrepo, M. R.; Mikhailova, E.; Bayley, H. *Proc Natl Acad Sci USA* **2008**, *105*, 19720-19725.

(18) Gu, L. Q.; Cheley, S.; Bayley, H. *Proc. Natl. Acad. Sci. U. S. A.* **2003**, *100*, 15498-15503.

(19) Li, T.; Liu, L.; Li, Y.; Xie, J.; Wu, H. C. *Angew. Chem. Int. Ed.* **2015**, *54*, 7568-7571.

(20) Wang, G.; Wang, L.; Han, Y.; Zhou, S.; Guan, X. *Biosens. Bioelectron.* **2014**, *53*, 453-458.

(21) Ho, C. W.; Meervelt, V. V.; Tsai, K. C.; Temmerman, P.-J. D.; Mast, J.; Maglia, G. *Sci. Adv.* **2015**, *1*, e1500905.

(22) Ying, Y. L.; Wang, H. Y.; Sutherland, T. C.; Long, Y.-T. *Small* **2011**, *7*, 87-94.

(23) Margulies, M.; Egholm, M.; Altman, W. E.; Attiya, S.; Bader, J. S.; Bemben, L. A.; Berka, J.; Braverman, M. S.; Chen, Y.-J.; Chen, Z.; et al. *Nature* **2005**, *437*, 376.

(24) Pebay-Peyroula, E.; Dahout-Gonzalez, C.; Kahn, R.; Trézéguet, V.; Lauquin, G. J.-M.; Brandolin, G. *Nature* **2003**, *426*, 39-44.

(25) de Britto, D.; Assis, O. B. *Carbohydr. Polym.* **2007**, *69*, 305-310.

(26) Crini, G. *Chem. Rev.* **2014**, *114*, 10940-10975.

(27) Chetnani, B.; Das, S.; Kumar, P.; Surolia, A.; Vijayan, M. *Acta Crystallogr. D Biol. Crystallogr.* **2009**, *65*, 312-325.

(28) Wang, Y.; Zhang, Y.; Guo, Y.; Kang, X. *Sci. Rep.* **2017**, *7*, 183.

(29) Kang, X.; Gu, L. Q.; Cheley, S.; Bayley, H. *Angew. Chem. Int. Ed.* **2005**, *44*, 1495-1499.

(30) Say, J.; Ciuffi, K.; Furriel, R. P.; Ciancaglini, P.; Leone, F. A. *Biochim. Biophys. Acta BBA-Gen. Subj.* **1991**, *1074*, 256-262.

(31) Kumar, S.; Tao, C.; Chien, M.; Hellner, B.; Balijepalli, A.; Robertson, J. W. F.; Li, Z.; Russo, J. J.; Reiner, J. E.; Kasianowicz, J. J.; et al. *Sci. Rep.* **2012**, *2*, 684.

(32) Wu, W.; Hu, H.; Li, F.; Wang, L.; Gao, J.; Lu, J.; Fan, C. *Chem. Commun.* **2011**, *47*, 1201-1203.

(33) Xu, F.; Cohen, S. N. *Nature* **1995**, *374*, 180-183.

(34) Ubersax, J. A.; Ferrell Jr, J. E. *Nat. Rev. Mol. Cell Biol.* **2007**, *8*, 530-541.

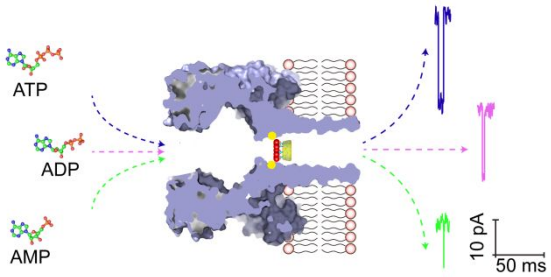
ATP
ADP
AMP
10 pA
50 ms